In situ chemical composition measurement of individual cloud residue particles at a mountain site, South China

Qinhao Lin[1,2], Guohua Zhang[1], Long Peng[1,2], Xinhui Bi[1,*], Xinming Wang[1], Fred J. Brechtel[3], Mei Li[4], Duohong Chen[5], Ping'an Peng[1], Guoying Sheng[1], Zhen Zhou[4]

[1] State Key Laboratory of Organic Geochemistry and Guangdong Key Laboratory of Environmental Protection and Resources Utilization, Guangzhou Institute of Geochemistry, Chinese Academy of Sciences, Guangzhou, 510640, PR China

[2] University of Chinese Academy of Sciences, Beijing, 100049, PR China

[3] Brechtel Manufacturing Inc., Hayward, 94544, California, USA

[4] Atmospheric Environment Institute of Safety and Pollution Control, Jinan University, Guangzhou 510632, PR China

[5] State Environmental Protection Key Laboratory of Regional Air Quality Monitoring, Guangdong Environmental Monitoring Center, Guangzhou 510308, PR China

* Correspondence to: Xinhui Bi (bixh@gig.ac.cn)

Tel.: +86-20-85290195

Highlights

1. EC-containing particles were the largest fraction of the total cloud residues (49.3% by number), dominating in the range of 0.2-1.0 μm.

2. The Nf of the cloud residue types was influenced by air mass chemistry.

3. Amine particles represented from 0.2% to 15.1% by number of the total cloud residues when air masses changed from northerly to southwesterly.

4. Compared with non-activated particles, nitrate intensity decreased in cloud residues except dust type.

Abstract

To investigate how atmospheric aerosol particles interact with chemical composition of cloud droplets, a ground-based counterflow virtual impactor (GCVI) coupled with a real-time single-particle aerosol mass spectrometer (SPAMS) was used to assess the chemical composition and mixing state of individual cloud residue particles in the Nanling Mountain Range (1,690 m a.s.l.), South China, in Jan 2016. The cloud residues were classified into nine particle types: Aged elemental carbon (EC), Potassium-rich (K-rich), Amine, Dust, Pb, Fe, Organic carbon (OC), Sodium-rich (Na-rich) and Other. The largest fraction of the total cloud residues was the Aged EC type (49.3% by number), followed by the K-rich type (33.9% by number). Abundant Aged EC cloud residues that mixed internally with inorganic salts were found in air masses from northerly polluted areas. The number fraction (Nf) of the K-rich cloud residues increased within southwesterly air masses from fire activities in Southeast Asia. When air masses changed from northerly polluted areas to southwesterly ocean and livestock areas, the Amine particles increased from 0.2% to 15.1% of the total cloud residues by number. The Dust, Fe, Pb, Na-rich and OC particle types had a low contribution (0.5-4.1% by number) to the total cloud residues. Higher fraction of nitrate (88-89% by number) was found in the Dust and Na-rich cloud residues relative to sulfate (41-42%) and ammonium (15-23%). Higher intensity of nitrate was found in the cloud residues relative to the ambient particles. Compared with non-activated particles, nitrate intensity decreased in cloud residues except dust type. To our knowledge, this study is the first report on in situ observation of the chemical composition and mixing state of individual cloud residue particles in China.

Keywords: GCVI, SPAMS, cloud residues, mixing state, South China

1 Introduction

Aerosol-cloud interactions influence the thermodynamic and radiation balance of the atmosphere (IPCC, Boucher et al., 2013). Anthropogenic particles can increase number concentration of small cloud droplets, and, in turn, affect reflectivity and life time of clouds (Stier et al., 2005; Lohmann et al., 2007; Rosenfeld et al., 2008). In situ cloud chemical measurements have shown varied chemical composition of cloud water or residues at various regions (Sorooshian et al., 2007a; Roth et al., 2016; Li et al., 2017). Despite a large number of aerosol/cloud studies over the past 20 years, the uncertainty for evaluating radiative forcing due to aerosol-cloud interactions has not been reduced (Seinfeld. et al., 2016). Therefore, it is crucial to assess how atmospheric aerosol particles contribute and interact with cloud droplets.

The ability of aerosol particles to act as cloud condensation nuclei (CCN) is dependent on the size and chemical composition of particles at a given supersaturation (McFiggans et al., 2006). Wiedensohler et al. (2009) found that the enhancement of particles CCN ability was related to an increase in the average sulfate mass concentration. Dusek et al. (2006) demonstrated that CCN behavior was more effected by aerosol size than chemical composition. Meanwhile, aerosol mixing state also play an important role in the ability of aerosol to act as CCN. It has been reported that freshly emitted elemental carbon (EC) particles generally exhibit low CCN activity, whereas aged EC particles show high CCN activity after experienced atmospheric processes (Zhang et al., 2008). Pratt et al. (2011) found that number fractions of ammonium or oxalate internally mixed with biomass

burning particles increased with an aged time of 81-88 min, which promote CCN behavior. Laboratory studies have shown that low-solubility organic particles internally mixed with ammonium sulfate would suppress water uptake of mixed particle and thus might affect CCN activity (Wise et al., 2003; Svenningsson et al., 2006; Sjogren et al., 2007). An over prediction of CCN concentration by up to 35% was estimated based on particle internal mixing state assumption (Medina et al., 2007; Collins et al., 2013). The influence of mixing state on aerosol CCN activity varies depending on the proximity to the pollution plume source and/or photochemical ageing activity (Ervens and Volkamer, 2010). More detailed measurements to characterize the mixing state of CCN particles would improve our understanding of aerosol-cloud interactions.

The combined technique of a counterflow virtual impactor (CVI) and an Aerosol Mass Spectrometer (AMS) or other online/offline single particle instruments is widely used to characterize the chemical composition and/or mixing state of cloud/fog droplet residue particles. These studies were mainly conducted in North America including Wyoming (Pratt et al., 2010a), Ohio (Hayden et al., 2008), Oklahoma (Berg et al., 2009), Florida (Cziczo et al., 2004; Twohy et al., 2005), California (Coggon et al., 2014), Europe including Schmücke (Roth et al., 2016; Schneider et al., 2017), Jungfraujoch (Kamphus et al., 2010), Åreskutan (Drewnick et al., 2007), Scandinavia (Targino et al., 2006), Arctic (Zelenyuk et al., 2010), Central America (Cziczo et al., 2013), West Africa (Matsuki et al., 2010) and marine areas (Twohy and Anderson 2008; Twohy et al., 2009; Shingler et al., 2012).

Over the past three decades, China has undergone rapid economic growth accompanied by increased aerosol emissions. Although scientists have worked to increase our

understanding of an emissions inventory and the temporal and spatial variation of atmospheric aerosols in China (Zhang et al., 2012b), only few studies have employed direct observation of the chemical composition and mixing state of cloud/fog droplets. Li et al. (2011b) utilized transmission electron microscopy to obtain the mixing state of individual ambient particles during cloud events at Mt. Tai in northern China. This result showed that sulfate-related salts dominated in larger particles. Bi et al. (2016) used a ground-counterflow virtual impactor (GCVI) coupled with a real-time single particle aerosol mass spectrometer (SPAMS) to explore the chemical composition and mixing state of individual fog residual particles at ground level in an urban area of South China. They found an abundance of EC-containing particles in fog residues.

Here, we present a study on the chemical composition and mixing state of individual cloud residue particles at a mountain site in South China. The same experimental methods of Bi et al. (2016) were used in this study. The size distribution, chemical composition and mixing state of cloud residues during cloud events are discussed. Moreover, the chemical compositions of ambient and non-activated particles were also compared with the cloud residues. The aim of this study is to assess the potential effects of anthropogenic aerosols from regional transportation on cloud formation and to investigate the dominant particle types in cloud droplets at a mountain site in South China.

2 Experimental

2.1 Measurement site

Our measurements were carried out during 15-26 Jan, 2016. The sampling site was located in the Nanling Background Station (112 °53’ 56” E, 24° 41’ 56” N, 1,690 m a.s.l.)

120 at the National Air Pollution Monitoring System in South China (Figure S1). This station
121 is located at 200 km north of the metropolitan city Guangzhou and 350 km north of the
122 South China Sea (Figure S1). This site is also surrounded by a national park forest (273
123 km^2), where there are scarcely any emissions from anthropogenic activities. During the
124 winter monsoon period, air pollution from northern China moves to southern China and
125 crosses the study region (Lee et al., 2005).
126
127 **2.2 Instrumentation**
128 In this study, a GCVI inlet system (GCVI Model 1205, Brechtel Mfg. Inc.) was used to
129 sample cloud droplets with a diameter greater than 8 μm. The ambient temperature on
130 average was 6.9 ℃ (ranging from -7.2 to 11.4 ℃) during cloud events. Only 20 cloud
131 residues that accounted for 0.08% of the total cloud residues were detected when the
132 ambient temperature was below -7 ℃ observed from 06:00 to 08:00 on 23 Jan. Thus,
133 cloud droplets were dominated by liquid water droplets. The measurements of the droplet
134 size spectra in this region performed during the winter of 1999-2001 showed that size of
135 cloud droplets ranged from 4 to 25 μm with average size of 10 μm and a corresponding
136 liquid water content of 0.11-0.15 g m^{-3} (Deng et al., 2007). Previous study in other
137 mountain site also showed an average size at ~10 μm (Borys et al., 2000). Hence,
138 assuming that size distribution of cloud droplets mostly was above 8 μm in this region.
139 The sampled cloud droplets were passed through an evaporation chamber (air flow
140 temperature at 40 ℃), where the associated water was removed and the dry residue
141 particles (with the air flow RH lower than 30%) remained. A stream of filtered and
142 heated ambient air (counterflow) was provided by a compressor. The particle

transmission efficiency of the cut size (8 μm) was 50%. The enrichment factor of the particles collected by the GCVI inlet was estimated to be 5.25 based on theoretical calculation (Shingler et al., 2012). Ambient particles were collected through an ambient inlet with a cut-off aerodynamic diameter (d_a) of 2.5 μm when cloud-free periods were present. Non-activated (interstitial) particles were sampled through the ambient inlet during the cloud events in this study. The ambient or non-activated particles inlet was dried using a silica gel diffusion dryer. During cloud-free periods, a ratio of particle concentration measured behind the CVI (below 1 cm^{-3}) to ambient aerosol concentration (2,000 cm^{-3}) was 0.0005, indicating that instances of particle breakthrough and small particle contamination were absent. The cloud droplet residues, ambient or non-activated particles were subsequently analyzed by a suite of aerosol measurement devices, including a SPAMS (Hexin Analytical Instrument Co., Ltd., Guangzhou, China), a scanning mobility particle sizer (SMPS) (MSP Cooperation) and an aethalometer (AE-33, Magee Scientific Inc.).

A detailed operational principle of the SPAMS has been described elsewhere (Li et al., 2011a). Briefly, aerosol particles are drawn into SPAMS through a critical orifice. The particles are focused and aerodynamically sized by two continuous diode Nd:YAG laser beams (532 nm). The particles are subsequently desorbed/ionized by a pulsed laser (266 nm) triggered exactly based on the velocity of the specific particle. The positive and negative ions generated are recorded with the corresponding size of individual particles. Polystyrene latex spheres (Nanosphere Size Standards, Duke Scientific Corp., Palo Alto) of 0.2-2.0 μm in diameter were used to calibrate the sizes of the detected particles. The ambient pressure was 830 hPa (826-842 hPa) during the measurements and the

calibration. Particles measured by SPAMS mostly fell within the size range of d_{va} 0.2-2.0 μm (Li et al., 2011a).

2.3 Definition of cloud events

To reliably identify the presence of cloud events, an upper-limit visibility threshold of 5 km and a lower-limit relative humidity (RH) threshold of 95% were set in the GCVI software (Bi et al., 2016). Three long-lasting cloud events occurred during the periods of 16:00 (local time) 15 Jan - 07:00 17 Jan (cloud I), 20:00 18 Jan - 12:00 19 Jan (cloud II) and 17:00 19 Jan - 13:00 23 Jan (cloud III), as marked in Figure 1. In addition, a cloud event occurred at 14:40 - 15:00 on 17 Jan, but we did not do an analysis due to the short duration. The measured cloud residual concentration was integrated by the SMPS and was then corrected by the enrichment factor and transmission efficiency of the GCVI. The corrected cloud residual concentrations on average were 436 cm^{-3}, 568 cm^{-3} and 544 cm^{-3} for cloud I, cloud II and cloud III, respectively (Figure S2). From 10:00 21 Jan to 13:00 23 Jan, cloud residues and non-activated particles were alternately sampled with an interval of one hour. During this period, a ratio of number residues to total number particles (sum of cloud residues and non-activated particle) on average was 0.43±0.20. Low levels of $PM_{2.5}$ (~ 12.7 μg m^{-3}) exclude the influence of hazy days. A rainfall detector of the GCVI system was also used to exclude rain droplet contamination. When cloud events occurred without precipitation, sampling was automatically triggered by the GCVI control software (Bi et al., 2016).

2.4 Particle classification

During this study period, a total of 73,996 particles including 49,322 ambient, 23,611 cloud residual and 1,063 non-activated particles with bipolar mass spectra were chemically analyzed in the size range of d_{va} 0.2-1.9 μm. The sampled particles were firstly classified into 101 clusters using an Adaptive Resonance Theory neural network (ART-2a) with a vigilance factor of 0.75, a learning rate of 0.05, and 20 iterations (Song et al., 1999). Then by manually combining similar clusters, eight major particle types Aged EC, Potassium-rich (K-rich), Amine, Dust, Fe, Pb, Organic carbon (OC), and Sodium-rich (Na-rich) with distinct chemical patterns were obtained, which represented ~99.9% of the population of the detected particles. The remaining particles were grouped together as "Other". Assuming that the number of individual particles followed Poisson distribution, standard errors for number fraction of particle type were estimated (Pratt et al., 2010a).

3 Results and discussion

3.1 Back trajectories and meteorological conditions

Back trajectories in this study were calculated using the Hybrid Single Particle Lagrangian Integrated Trajectory (HYSPLIT Model). A height of the HYSPLIT model in the study region (a spatial resolution of $0.5° \times 0.5°$) is averaged 500 m a.s.l., lower than height of the observed site (1,690 m a.s.l.). Thus, a height of 1,800 m a.s.l. (approximately 100 m above the observed site) was chosen as an endpoint in the model. The station was mainly affected by southwesterly or northerly air masses in this study (Figure 2). In addition, the beginning altitude of the southwesterly air masses traversed at

lower heights relative to the northerly air masses (Figure 2). The southwesterly air masses, accompanied by warm moist airflows, occurred during 15-17 and 20-21 Jan, which promoted high RH condition (Figure 1). Conversely, the northerly air masses, associated with cool dry airstreams, occurred during 18 and 23-24 Jan and led to a decrease in temperature and relative humidity. Note that, on 18-19 and 22-23 Jan, the air mass encountered initial mixing of northerly cloud-free air and southwesterly cloudy air. Entrainment of nuclei particles originated from northern air masses might be activated to cloud droplets (Sect. 3.4).

Meteorological conditions were unstable, with high southwesterly flow (~ 6.5 m s^{-1}) during 15-17 and 20-22 Jan (Figure 1). The level of $PM_{2.5}$ remained a low value of approximately 3 μg m^{-3} for this time period. A high level of $PM_{2.5}$ (~20 μg m^{-3}) was observed during 18 Jan when the northerly flow dominated. Similarly, the average $PM_{2.5}$ value reached 24 μg m^{-3} during 24 Jan. Although the local northerly and southwesterly flows occurred alternately, the particles were still originated from the northerly air mass for this period (Figure 2). During 23-24 Jan, a sharp decrease in temperature (Figure 1) was observed due to a cold wave associated with a violent northerly flow. The wind speed during the cold wave exceeded the upper-limit speed (~12 m/s) of a wind speed sensor.

3.2 The chemical characterization of cloud droplet residues

Figure 3 shows the average positive and negative mass spectra of the main six particle types. The Aged EC particles were characterized by EC cluster ions (e.g., m/z $\pm 12C^{+/-}$, $\pm 36C_3^{+/-}$, $\pm 48C_4^{+/-}$, $\pm 60C_5^{+/-}$, …) and a strong K^+ ion signal (m/z $39K^+$) as well as a

sulfate ion signal (m/z -97HSO_4^-), and some minor organic markers (m/z 27$C_2H_3^+$, 43$C_2H_3O^+$) (Moffet and Prather, 2009). EC particles mainly originated from combustion processes (Bond et al., 2013). The strong K^+ ion signal in the Aged EC particles implies partially originated from biomass burning sources (Bi et al. 2011). The Aged EC particle type was the largest fraction (49.3% by number) of the total cloud residues (Figure S3). In addition, number fraction (Nf) of the Aged EC residues significantly decreased from 54.1% in the size range of 0.2-1.0 μm to 19.2% in the size range of 1.1-1.9 μm (Figure 4). Note that the chemical composition of cloud residues is dependent on the particle size (Roth et al., 2016), and the number reported for each particle type might suffer from the bias related to size-dependent transmission efficiency (Qin et al., 2006). The relative fraction of cloud residues in 0.1 μm size interval is presented to minimize the influence of size-dependent transmission efficiency of single particle mass spectrometry (Roth et al., 2016).

The K-rich particles exhibited the highest peak at m/z 39K^+, mainly combined with sulfate and nitrate (m/z -46NO_2^-, -62NO_3^-) and presumably derived from biomass/biofuel burning source (Moffet et al., 2008; Pratt et al. 2011; Zhang et al., 2013). An aged time of 81-88 min biomass burning particles were found to show an increase in the mass fractions of ammonium, sulfate, and nitrate (Pratt et al. 2011). In this study, the K-rich particles would be expected to experience aged process due to strong sulfate and nitrate signals (Hudson et al. 2004; Pratt et al. 2011). Aged biomass burning particles can participate in cloud droplets formation and show an effective CCN activity (Pratt et al. 2010a). The K-rich particle type, the second largest contributor, accounted for 33.9% by number of the total cloud residues (Figure S3).

The abundant aged soot/EC and biomass burning particles were often detected in cloud residues (Pratt et al., 2010a; Roth et al., 2016). The contribution of local anthropogenic origins to aged soot and/or biomass burning particles in cloud/fog residues has been reported in Schmücke (Roth et al., 2016) and Guangzhou city (Bi et al., 2016). At the North Slope of Alaska, the measurement of biomass burning particles in cloud residues mainly resulted from local vicinity or as far away as Siberia and Asian sources (Zelenyuk et al., 2010; Hiranuma et al., 2013). Similarly, the majority of Aged EC and K-rich cloud residues observed here are expected to originate from long-range transportation due to insignificant sources of local anthropogenic emissions and the fire dots (Figure 2). At the Jungfraujoch station (3,580 m a.s.l.) in Europe, the K-rich (biomass burning) particles only contributed 3% of the cloud droplets, and the Aged EC residuals were insignificant (<1% by number) (Kamphus et al., 2010). The Jungraujoch station is predominantly within the free tropospheric condition, such that the biomass burning contribution can be expected to be lower than at other sites.

The Amine particles were characterized by related amine ion signals at m/z $58C_2H_5NHCH_2^+$ (diethylamine, DEA), $59N(CH_3)_3^+$ (trimethylamine, TMA) and $86C_5H_{12}N^+$ (triethylamine, TEA) (Angelino et al., 2001; Moffet et al., 2008). This particle type also contained sulfuric acid ion signals at m/z $-195H(HSO_4)_2^-$, indicative of acidic particles (Rehbein et al., 2011). The Amine particles represented 3.8% by number of the total cloud residues (Figure S3). Higher Nf of the Amine residues was detected in the size range from 0.7 to 1.9 μm relative to the size range from 0.2 to 0.6 μm (16.7% versus 0.4%), as shown in Figure 4. Aqueous reactions improving the participation of amine have been observed in Guangzhou (Zhang et al., 2012a) and Southern Ontario

(Rehbein et al., 2011). A recent study also showed a clear enhancement of amine-containing particles in cloud residues compared to the ambient particles (9% versus 2% by number) (Roth et al., 2016). It indicates a preferential formation of amine within the cloud, which is in contrast to the observations of Bi et al. (2016). It might suggests that enhancement of particle amine is not only depend on high RH or fog/cloud process, but also sensitive to other parameters, such as presence of gas phase amine source (Rehbein et al., 2011).

The Dust particles presented significant ions at m/z $40Ca^+$, $56CaO^+/Fe^+$, $96Ca_2O^+$ and $-76SiO_3^-$ and sulfate as well as nitrate markers. Previous studies showed that dust particles that are internally mixed with sulfate and nitrate are expected to act as CCN (Twohy and Anderson 2008; Twohy et al., 2009), despite sulfate and nitrate partial formation from in-cloud production. This type contributed 2.9% by number of the total cloud residues (Figure S3). A slight increase in Nf of the Dust residues was observed in size range above 0.5 μm relative to that below 0.5 μm (3.0% versus 1.0% by number). At Mt. Tai in northern China, a high concentration of Ca^{2+} in cloud/fog water was mainly attributed to a sandstorm event during the spring season (Wang et al., 2011). At Mt. Heng in southern China, the abundant crust-related elements (e.g., Al) observed in cloud water is due to Asian dust storms that occurred in March-May (Li et al., 2017). Based on the backward trajectory, the site was unlikely affected by sandstorm source in northwestern China during the cloud events. Local dust emissions by anthropogenic-disturbing soils or removing vegetation cover can be excluded as a result of forest protection. Additionally, dust residues may have occupied larger CCN (Tang et al., 2016), which cannot be

303 detected by the SPAMS. Hence, a low fraction (2.9% by number) of dust cloud residue
304 might be due to the limitation of the SPAMS.

305 The Fe particles had its typical ions at m/z 56Fe^+ and internally mixed with sulfate
306 and nitrate, made up 4.1% by number of the total cloud residues. Approximately 16% of
307 the Fe cloud residues contained Ca^+ peak (m/z 40). Predominant Fe ion peaks possibly
308 indicates the contribution from anthropogenic sources (Zhang et al., 2014), especially the
309 northern air masses across iron/steel industrial activities in Yangtze River Mid-Reaches
310 city clusters (Figure 2). The contribution of anthropogenic and natural Fe-containing
311 particles sources (Moteki et al., 2017) to observed Fe-containing residues is expected.
312 The presence of Fe in the cloud droplets play an important role in aqueous-phase SO_2
313 catalytic oxidation in cloud processing (Harris et al., 2013), thus accelerating the sulfate
314 content of Fe-containing particles in cloud processing.

315 The Na-rich particles were mainly composed of ion peaks at m/z 23Na^+ and 39K^+ in
316 the positive mass spectra, and nitrate and sulfate species in the negative mass spectra,
317 made up 3.0% by number of the total cloud residues. Na-rich particles are formed from
318 varied sources including industrial emissions, sea salt or dry lake beds (Moffet et al.
319 2008). The Nf of Na-rich cloud residues did not increase from continental (Northerly) air
320 mass on 19 Jan to maritime (southwesterly) air mass on 21 Jan (3.3% versus 2.4% by
321 number). However, the related sea salt ion peak area (m/z, 81/83 $Na_2{}^{35}Cl^+/Na_2{}^{37}Cl^+$) were
322 enhanced for Na-rich particles origination from maritime air mass relative to continental
323 air mass (3.8 $\pm$ 2.4 times). The continental air masses crossed industrial areas where the
324 Yangtze River Mid-Reaches city cluster is located (Figure 2). Industrial emissions were a
325 possible contributor to Na-rich particles under the influence of continental air masses

(Wang et al. 2016). This might suggest that the Na-rich particles were originated from both industrial emissions and sea salts.

The OC, Pb and Other particle types contributed 0.1%-2.3% by number to the total cloud residues (Figure S3). Their average mass spectra can be found in Figure S4. The OC particles presented dominant intense OC signals (e.g., m/z $27C_2H_3^+$, $37C_3H^+$, $43C_2H_3O^+$ and $51C_4H_3^+$) and abundant sulfate. Presence of K^+ signal was found in the OC particles, suggesting possible biomass burning sources (Bi et al. 2011). OC particles might exist in smaller cloud residues (Sellegri et al., 2003a), which cannot be detected by the SPAMS. The Pb particles showed its typical ions at m/z $208Pb^+$ and internally mixed with K^+ and Cl^-. Previous studies have found that K and Cl internally mixed with Pb particles have a possible origination of waste incineration (Zhang et al., 2009) or iron and steel products manufacturing facilities (Tsai et al., 2007). Only three particles were found containing calcium, organic carbon, organic nitrogen and phosphate ion signals, implying a possible existence of biological particles (Pratt et al., 2009a). Such particles were classified as the Other type due to low number.

Previous measurements have found that dust, playa salts, sea salt or metal particles were often enriched in larger cloud droplets (~20 μm) (Bator and Collett, 1997; Moore et al., 2004; Pratt et al., 2010b). Organic carbon tended to be enriched in small cloud/fog droplets, extending to 4 μm (Herckes et al., 2013). The size of cloud droplets were above 8 μm in the present study. Additionally, the particle transmission efficiency increased with increasing cloud droplet size (Shingler et al., 2012). Thus, it partially leads to relatively larger fractions of the observed Dust, Na-rich and metal cloud residues, and the less fraction of the OC cloud residues in this study.

3.3 Mixing state of secondary species in cloud residues

The high Nfs of sulfate-containing particles were found in the K-rich (91%), OC (100%), Aged EC (98%), Pb (74%), Fe (93%) and Amine (99%) cloud residues, as shown in Figure 5. Lower Nfs of sulfate-containing particles were observed in the Na-rich (41%) and Dust (42%) cloud residues. In contrast, nitrate-containing particles contributed 89% and 88% by number to the Na-rich and Dust cloud residues, respectively. The acid displacement reaction of sea salt chloride (Na-rich particles) by HNO_3 might lead to a depletion of chloride and enhancement of nitrate (Laskin et al., 2012). Similarly, the heterogeneous chemistry of HNO_3 in the dust particles also contributes the preferential enrichment of nitrate (Tang et al., 2016). Moreover, after activation, uptake of gas-phase HNO_3 would increase nitrate level in the cloud residues (Schneider et al., 2017). The nitrate in the cloud residues was thought to be in the form of ammonium nitrate by estimating the ratio of m/z 30 to m/z 46 in AMS data (Drewnick et al., 2007; Hayden et al., 2008). Relative to nitrate, low portions of ammonium (m/z, $18NH_4^+$) in the Na-rich (23% by number) and Dust (15% by number) cloud residues suggest that in this region, ammonium nitrate was not a predominant form of nitrate in the two cloud residual types. The Na-rich and Dust types were mainly composed of alkaline ion peaks (m/z, $23Na^+$, $39K^+$ and $40Ca^+$) in position mass spectra (Figure 3), accompanied with larger fraction (88-89%) of nitrate. Thus, our data suggests that nitrate might exist in the form of $Ca(NO_3)_2$, $NaNO_3$ or KNO_3 in the Dust and Na-rich cloud residues. It should be noted that the evaporation chamber of the GCVI may lead to a reduction of ammonium nitrate in the cloud residues (Hayden et al., 2008). The nitrate-containing particles accounted for only 46% by number of the Aged EC cloud residues, which is significantly less than the

sulfate-containing particles. Previous field studies have found that Aged EC (soot) fog/cloud residues are mainly internally mixed with sulfate (Pratt et al., 2010a; Harris et al., 2014; Bi et al., 2016). Aged EC particles mixed with sulfate are good CCN, rather than formed by in-cloud processing (Bi et al., 2016; Roth et al., 2016). Laboratory measurements have also demonstrated that EC particles internally mixed with sulfate showed a high hygroscopic behavior and thus affect CCN ability (McMeeking et al., 2011). High portions (75-86% by number) of ammonium-containing particles were observed for the OC and Aged EC cloud residues, suggesting that ammonium will mostly be in the form of ammonium sulfate or ammonium nitrate for two cloud residual types (Zhang et al., 2017). This result also implies that ammonium-containing particles are preferentially activated or enhanced uptake of gaseous NH_3 to neutralize acidic cloud droplets for the OC and EC types.

Water soluble organics (e.g., amine and oxalate) have previously been measured in cloud water/residues (Sellegri et al., 2003b; Sorooshian et al., 2007a; Pratt et al., 2010a). The presence of TMA (93% by number) in the Amine cloud residues is expected to promote water uptake activity (Sorooshian et al., 2007b). A total of 3,410 oxalate-containing particles (m/z, -89$HC_2O_4^-$) represented 14.4% by number of the total cloud residues, which was mainly associated with the K-rich cloud residues (~70% by number). Oxalate-containing particles (~30% by number) in the metal (Pb, Fe) cloud residues might be in the form of metal oxalate complexes from reactions of in-cloud formation oxalate with metals (Furukawa and Takahashi, 2011). Oxalate can readily partition into the particle phase to form amine salts (Pratt et al., 2009b). It may facilitate the entrainment of oxalate (33% by number) in the Amine residues. A low fraction (4%) of

oxalate-containing particles in the OC type is a result of restrictive classification. Classification of the OC particles is mainly based on intense organic carbon ion signals (e.g., m/z 27$C_2H_3^+$, 37C_3H^+, 43$C_2H_3O^+$ and 51$C_4H_3^+$).The majority of oxalate-containing particles were internally mixed with the K-rich type. Therefore, oxalate was classified to the K-rich type and probably contributed from biomass burning. The K-rich particles could contain an abundant of organics (Pratt et al. 2011), however, the signals of organics were covered by the potassium due to its high sensitivity to the laser.

3.4 Comparison of cloud residues in different air mass sources

Figure 6 displays the hourly detected particle counts and Nf values of the nine types of cloud residues and ambient particles. The Nf of the Aged EC type showed a very abrupt increase from cloud residues to ambient particles on Jan 17. The ambient RH showed an abrupt decrease from nearly 100% at 10:00 to 85% at 11:00 on 17 Jan (Figure 1). The ambient temperature also decreased from 10 ℃ at 11:00 to 4 ℃ at 18:00 on 17 Jan (Figure 1). These changes imply that the air mass shifted from southwesterly cloudy air to northerly cloud-free air around noon on 17 Jan (Figure 2). The entrained particles originated from northern air mass might have insufficient supersaturation to be activated as cloud droplets. It resulted in the remarkable increase of the Aged EC particles in ambient particles on Jan 17 (Figure 6).

The ambient RH increased from 60% at 19:00 to nearly 100% at 21:00 on 18 Jan (Figure 1). The ambient temperature also increased from 1.3 ℃ at 22:00 on 18 Jan to 3.2 ℃ at 06:00 on 19 Jan (Figure 1). These changes imply that the air mass changed from northerly cloud-free air to southwesterly cloudy air at night on 18 Jan (Figure 2). During

18-19 Jan, the cloud residues and ambient particles showed similar chemical characteristics and were dominated by Aged EC particles (Figure 6). A lack of significant variation in the particle types for this period suggests that nuclei particles originated from northerly cloud-free air could be activated to become cloud droplets. When a cloud-free event occurred at 11:00-17:00 on 19 Jan, ambient particles remained a high level of $PM_{2.5}$ (~ 22.7 μg m^{-3}). The southwesterly wind flow on 19-20 Jan was too weak (~ 2.75 m s^{-1}) to dilute particles originated from the northerly air masses (Figure 1). Additionally, a high RH (90%) air mass at height 1,500 m (a.s.l.) gradually moved to northern China from 19 to 20 Jan (Figure S5). These changes might have led to similar residual particle types observed from 19 Jan to 20 Jan, although the site encountered southwesterly cloudy air on 19-20 Jan (Figure 2).

As mentioned above, the Nf of the cloud residue types significantly changed as the air mass origin varied from northerly to southwesterly. To further investigate the influence of air mass history, we selected to analyze cloud residues that had arrived from a northerly air mass on 18-19 Jan as compared to cloud residues that originating from a southwesterly air mass during the periods of 16-17 and 21-22 Jan. The detected number of cloud residues for both the northerly and southwesterly air masses are given in Table S1. The southwesterly air masses accompanied by high relative humidity (90%) (Figure S5) may have triggered particles activated to CCN prior to their arrival to the sampling site.

The K-rich type was found to contribute 23.9% to the cloud residues in the northerly air mass, which was significantly lower than its contribution to the southwesterly air mass (51.5%), as shown in Figure 7. A similarity in averaged mass spectrum of the K-rich

residues was found for the southwesterly and northerly air masses (Figure S6). The considerable increase of K-rich cloud residues suggests a major influence of regional biomass-burning activities. Biomass-burning emissions from Southeast Asia, including Myanmar, Vietnam, Laos and Thailand, where abundant fire dots are observed (Figure 2), could have been transported to the sampling site under a southwesterly air mass (Duncan et al., 2003). In contrast, the Aged EC type represented only 23.7% of the cloud residues under the influence of the southwesterly air mass, which was significantly lower than observations for the northerly air mass (59.9%), as shown in Figure 7. This result suggests that the northern air mass has a greater influence on the presence of Aged EC cloud residues.

An obvious increase in Nf of the Amine type was observed in the southwesterly air mass (15.1%) compared to the northerly air mass (0.2%), as shown in Figure 7. This data implies that the sources or formation mechanisms of amine in cloud residues varied in different air masses. The southwesterly air masses arrived from as far as the Bay of Bengal and then travelled through Southeast Asia region before reaching South China (Figure 2). The potential gas amine emissions from ocean (Facchini et al., 2008) and livestock areas (90 million animals, data was available at the website http://faostat3.fao.org) in Southeast Asia region might promote the enrichment of amine particles. Furthermore, after activation, the partitioning of the gas amine on cloud droplets may further contribute to the enhanced Amine cloud residues (Rehbein et al., 2011), especially for air masses delivered via routes with high relative humidity, as mentioned above (Figure S5). In contrast, northerly air mass accompanied with dry

463 airstreams may unfavorably induce the partitioning of gas amines into the particle phase
464 (Rehbein et al., 2011).
465
466 **3.5 Comparison of cloud residues with ambient and non-activated particles**
467 A direct comparison between cloud residues and ambient particles was limited because of
468 their differences in air mass origins. During the sampling period, the cloud events
469 occurred once the southwesterly air masses were dominant. Hence a comparison between
470 cloud residues and ambient particles cannot be addressed under the influence of
471 southwesterly air masses. Here, we chose five hours before and after the beginning of the
472 cloud II period in order to compare cloud residues and ambient particles with similar
473 northerly air mass origins, as discussed in Sect. 3.4.
474 The cloud residues and non-activated particles were alternately sampled with an
475 interval of one hour from 21 Jan to 23 Jan. The ambient temperature decreased from 6 ℃
476 at 11:00 to 0 ℃ at 23:00 on 22 Jan (Figure 1). Ambient particles level (sum of residual
477 and non-activated particles) showed a clearly increase from 156 cm^{-3} to 1460 cm^{-3} during
478 this period (Figure S2). Thus, the data suggests that the initial mixing of northerly cloud-
479 free air and southwesterly cloudy air occurred around noon on 22 Jan. A reduction of
480 supersaturation due to entrainment of the dry northern air mass might have insufficient
481 moisture to activate small particles, leading to unactivated particles above 0.2 μm
482 (Figure S7) (Mertes et al., 2005; Kleinman et al., 2012; Hammer et al., 2014), which can
483 be detected by the SPAMS.
484 The contribution of K-rich particles in cloud residues (23.9%) slightly decreased
485 relative to ambient particles (30.7%), as shown in Figure 7. Previous studies have found

that there were no significant changes in Nf of biomass-burning particles for cloud residues relative to ambient particles (Pratt et al., 2010a; Roth et al., 2016). The biomass-burning particles internally mixed with soluble species (e.g., sulfate, nitrate and oxalate) enhanced their ability to act as CCN, as discussed in Sect. 3.3. Kamphus et al. (2010) reported that biomass-burning particles account for only 3% of cloud residues compared with 43% of ambient particles, and they suspected that biomass-burning particles might exist in the form of tar balls (hydrophobic materials). A slight increase in Nf of the Aged EC cloud residues (59.9%) was observed relative to ambient particles (53.8%), as shown in Figure 7. In general, freshly emitted EC particles are less hydrophilic and are not active as CCN (Bond et al., 2013). The Aged EC particles show a high degree of internal mixing with secondary inorganic compounds in this study (Figure 5), improving their ability to act as CCN. The remaining particle types showed no clear differences in Nf between cloud residues and ambient particles.

When comparing the cloud residues with non-activated particles, a significant change in Nf was found for the Aged EC and K-rich type. A higher Nf of K-rich particles and a lower Nf of EC particles were found for the cloud residues relative to the non-activated particles (Figure 7). Entrainment of northerly cloud-free air might lower supersaturation during this period. Aged EC particles may require very high supersaturation to grow into cloud droplets and thus, only form hydrated non-activated aerosol (Hallberg et al., 1994).

Figure 8 and 9 show the differences in average mass spectra for cloud residues versus ambient particles, as well as cloud residues versus non-activated particles, respectively. Nitrate intensity (average ion peak area) enhanced in the cloud residues when compared to ambient particles. In addition, nitrate-containing particles accounted

for 70% of the cloud residues compared to 38% of the ambient particles. Drewnick et al. (2007) suggested that rather than sulfate, high nitrate content in pre-existing particles preferentially acted as cloud droplets. Compared with nitrate-containing ambient particles, larger size of containing-nitrate residues (Figure S8) possibly reflect the uptake of gaseous HNO_3 during cloud process (Hayden et al. 2008; Roth et al., 2016). A recent study also confirmed that the update of gaseous HNO_3 is an important contributor for the increased nitrate level in the cloud residuals (Schneider et al., 2017). Interestingly, we observed a decrease in nitrate intensity in cloud residues except dust type (Figure 9), and a large size distribution of nitrate-containing cloud residues (Figure S7) when compared with non-activated particles. This result suggests that particle size, rather than nitrate content, plays a more important role in the activation of particles into cloud droplets.

Sulfate intensity enhancement was only observed in the OC cloud residues relative to both ambient and non-activated particles. Although the in-cloud addition of sulfate can be produced from aqueous Fe-catalyzed or oxidation by H_2O_2/O_3 reactions (Harris et al., 2014), sulfate abundance was found in the Fe cloud residues relative to non-activated particles, but no enhancement relative to ambient particles. Previous studies also showed that the mass or number fraction of sulfate-containing particles in the cloud residues changed between ambient and non-activated particles (Drewnick et al., 2007; Twohy and Anderson, 2008; Schneider et al., 2017). However, the reason for these changes remains unclear.

The in-cloud process has been reported to be an important pathway for the production of amine particles (Rehbein et al., 2011; Zhang et al., 2012a). In this study, no remarkable change in Nf of the Amine cloud residues was obtained relative to the

ambient particles (0.2% versus 0.2% by number), as shown in Figure 7. The absence of amine species in cloud residues may be partially affected by droplet evaporation in the GCVI (Bi et al., 2016). However, there was a high fraction of the amine cloud residuals when the southwesterly air mass prevailed, as discussed in Sect. 3.4. A lack of gas-phase amines may be the cause of few amine particles detected in the ambient particles and cloud residues (Rehbein et al., 2011). An increase in Nf of cloud residues was observed compared with non-activated particles (5.2% versus 0.1% by number), as shown in Figure 7. An increase of particle water content facilitates partitioning of gas-phase amine species into the aqueous phase when gas-phase amines present (Rehbein et al., 2011).

4 Conclusions

This study presented an in situ observation of individual cloud residues, non-activated and ambient particles at a mountain site in South China. The finding shows that the Aged EC (49.3%) and K-rich types (33.9%) dominate the cloud residues in a remote area of China, followed by the Fe (4.1%), Amine (3.8%), Na-rich (3.0%) and Dust (2.9%) types. The OC, Pb and Other types contributed 0.1%-2.3% by number to the total cloud residues. The observed change in Nf of the cloud residue types, influenced by various air masses, highlights the important role of regional transportation in the observed cloud residual chemistry. Amine particles represented from 0.2% to 15.1% by number of the total cloud residues dependent on the air mass history. Sulfate was found to be highly mixed with the K-rich, OC, Aged EC, Pb, Fe and Amine cloud residues, while nitrate was highly mixed with the Na-rich and Dust cloud residues. Compared with non-activated particles, nitrate intensity decreased in cloud residues except dust type, and sulfate

555 intensity enhancement was only observed in the OC and Fe cloud residues.

556

557 **Acknowledgments**

558 This work was supported by the National Key Research and Development Program of
559 China (2017YFC0210100), the National Nature Science Foundation of China (No.
560 91544101 and 41405131) and the Foundation for Leading Talents of the Guangdong
561 Province Government. The authors thank Ji Ou from Shaoguan city Environmental
562 Monitoring Center for the help during the study. We also acknowledge the NOAA Air
563 Resources Laboratory (ARL) for the provision of the HYSPLIT transport and dispersion
564 model and/or READY website (http://ready.arl.noaa.gov) used in this publication. All the
565 data can be obtained by contacting the corresponding author.

566

567 **References**

568 Angelino, S., Suess, D.T. and Prather, K. A.: Formation of aerosol particles from
569 reactions of secondary and tertiary alkylamines: Characterization by aerosol time-of-
570 flight mass spectrometry, Environ. Sci. Technol., 35, 3130-3138, doi:
571 10.1021/es0015444, 2001.

572 Bator, A. and Collett, J.L.: Cloud chemistry varies with drop size, J. Geophys. Res.
573 Atmos., 102, 28071-28078, 1997.

574 Bi, X., Lin, Q., Peng, L., Zhang, G., Wang, X., Brechtel, F. J., Chen, D., Li, M., Peng, P.
575 a., Sheng, G. and Zhou, Z.: In situ detection of the chemistry of individual fog droplet
576 residues in the Pearl River Delta region, China, J. Geophys. Res. Atmos., 121(15),
577 9105-9116, doi:10.1002/2016jd024886, 2016.

578 Bi, X., Zhang, G., Li, L., Wang, X., Li, M., Sheng, G., Fu, J. and Zhou, Z.: Mixing state
579 of biomass burning particles by single particle aerosol mass spectrometer in the urban
580 area of PRD, China. Atmos. Environ., 45, 3447-3453,
581 doi:10.1016/j.atmosenv.2011.03.034, 2011.
582 Berg, L.K., Berkowitz, C.M., Hubbe, J.M., Ogren, J.A., Hostetler, C.A., Ferrare, R.A.,
583 Hair, J.W., Dubey, M.K., Mazzoleni, C. and Andrews, E.: Overview of the cumulus
584 humilis aerosol processing study, B. Am. Meteorol. Soc. 90, 1653-1667,
585 http://dx.doi.org/10.1175/2009BAMS2760.1, 2009.
586 Bond, T. C., Doherty, S. J., Fahey, D. W., Forster, P. M., Berntsen, T., DeAngelo, B. J.,
587 Flanner, M. G., Ghan, S., Kärcher, B., Koch, D., Kinne, S., Kondo, Y., Quinn, P. K.,
588 Sarofim, M. C., Schultz, M. G., Schulz, M., Venkataraman, C., Zhang, H., Zhang, S.,
589 Bellouin, N., Guttikunda, S. K., Hopke, P. K., Jacobson, M. Z., Kaiser, J. W., Klimont,
590 Z., Lohmann, U., Schwarz, J. P., Shindell, D., Storelvmo, T., Warren, S. G. and Zender,
591 C. S.: Bounding the role of black carbon in the climate system: A scientific assessment,
592 J. Geophys. Res. Atmos., 118, 5380-5552, doi:10.1002/jgrd.50171, 2013.
593 Borys, R. D., Lowenthal, D. H. and Mitchell, D. L.: The relationships among cloud
594 microphysics, chemistry, and precipitation rate in cold mountain clouds, Atmos.
595 Environ., 34(16), 2593-2602, 2000.
596 Boucher, O., Randall, D., Artaxo, P., Bretherton, C., Feingold, G., Forster, P., Kerminen,
597 V., Kondo,Y., Liao, H., Lohmann, U., Rasch, P., Satheesh, S., Sherwood, S., Stevens,
598 B. and Zhang X.: Clouds and Aerosols. In Climate Change 2013: The Physical Science
599 Basis. Contribution of Working Group I to the Fifth Assessment Report of the
600 Intergovernmental Panel on Climate Change [Stocker, T.F., D. Qin, G.-K. Plattner, M.

Tignor, S.K. Allen, J. Boschung, A. Nauels, Y. Xia, V. Bex and P.M. Midgley (eds.)]. Cambridge University Press, Cambridge, United Kingdom and New York, NY, USA. 2013.

Coggon, M.M., Sorooshian, A., Wang, Z., Craven, J.S., Metcalf, A.R., Lin, J.J., Nenes, A., Jonsson, H.H., Flagan, R.C. and Seinfeld, J.H.: Observations of continental biogenic impacts on marine aerosol and clouds off the coast of California, J. Geophys. Res. Atmos., 119, 6724-6748, doi:10.1002/2013JD021228, 2014.

Collins, D. B., Ault, A. P., Moffet, R. C., Ruppel, M. J., Cuadra‐Rodriguez, L. A., Guasco, T. L., Corrigan, C. E., Pedler, B. E., Azam, F., Aluwihare, L. I., Bertram, T. H., Roberts, G. C., Grassian, V. H. and Bertram, T. H.: Impact of marine biogeochemistry on the chemical mixing state and cloud forming ability of nascent sea spray aerosol, J. Geophys. Res. Atmos., 118(15), 8553-8565, 2013.

Cziczo, D.J., Murphy, D.M., Hudson, P.K. and Thomson, D.S.: Single particle measurements of the chemical composition of cirrus ice residue during CRYSTAL-FACE, J. Geophys. Res. Atmos., 109, D04201, doi:10.1029/2003JD004032, 2004.

Cziczo, D.J., Froyd, K.D., Hoose, C., Jensen, E.J., Diao, M., Zondlo, M.A., Smith, J.B., Twohy, C.H. and Murphy, D.M.: Clarifying the dominant sources and mechanisms of cirrus cloud formation, Science, 340, 1320-1324, doi: 10.1126/science.1234145, 2013.

Drewnick, F., Schneider, J., Hings, S. S., Hock, N., Noone, K., Targino, A., Weimer, S. and Borrmann, S.: Measurement of ambient, interstitial, and residual aerosol particles on a mountaintop site in central Sweden using an aerosol mass spectrometer and a CVI, J. Atmos. Chem., 56, 1-20, doi:10.1007/s10874-006-9036-8, 2007.

623 Deng, X., Wu, D., Shi, Y., Tang, H., Fan, S., Huang, H., Mao, W. and Ye, Y.:
624 Comprehensive analysis of the macro-and micro-physical characteristics of dense fog
625 in the area south of the Nanling Mountains (in Chinese), J.Trop. Meteorol., 23, 424-
626 434, 2007.
627 Duncan, B. N., Martin, R. V., Staudt, A. C., Yevich, R. and Logan, J. A.: Interannual and
628 seasonal variability of biomass burning emissions constrained by satellite observations,
629 J. Geophys. Res. Atmos., 108(D2), doi:108, 10.1029/2002jd002378, 2003.
630 Dusek, U., Frank, G., Hildebrandt, L., Curtius, J., Schneider, J., Walter, S., Chand, D.,
631 Drewnick, F., Hings, S. and Jung, D.: Size matters more than chemistry for cloud-
632 nucleating ability of aerosol particles, Science, 312, 1375-1378, 2006.
633 Ervens, B. and Volkamer, R.: Glyoxal processing by aerosol multiphase chemistry:
634 towards a kinetic modeling framework of secondary organic aerosol formation in
635 aqueous particles, Atmos. Chem. Phys., 10(17), 8219-8244, 2010.
636 Facchini, M. C., Decesari, S., Rinaldi, M., Carbone, C., Finessi, E., Mircea, M., Fuzzi, S.,
637 Moretti, F., Tagliavini, E. and Ceburnis, D.: Important source of marine secondary
638 organic aerosol from biogenic amines, Environ. Sci. Technol., 42, 9116-9121, doi:
639 10.1021/es8018385, 2008.
640 Furukawa, T. and Takahashi, Y.: Oxalate metal complexes in aerosol particles:
641 implications for the hygroscopicity of oxalate-containing particles, Atmos. Chem.
642 Phys., 11, 4289-4301, doi:10.5194/acp-11-4289-2011, 2011.
643 Hallberg, A., Ogren, J. A., Noone, K. J., Okada, K., Heintzenberg, J. and Svenningsson, I.
644 B.: The influence of aerosol particle composition on cloud droplet formation, J. Atmos.
645 Chem., 19, 153-171, doi: 10.1007/978-94-011-0313-8_8,1994.

Harris, E., Sinha, B., van Pinxteren, D., Tilgner, A., Fomba, K. W., Schneider, J., Roth, A., Gnauk, T., Fahlbusch, B. and Mertes, S.: Enhanced role of transition metal ion catalysis during in-cloud oxidation of SO_2, Science, 340, 727-730, doi:10.1126/science.1230911, 2013.

Harris, E., Sinha, B., van Pinxteren, D., Schneider, J., Poulain, L., Collett, J., D'Anna, B., Fahlbusch, B., Foley, S., Fomba, K. W., George, C., Gnauk, T., Henning, S., Lee, T., Mertes, S., Roth, A., Stratmann, F., Borrmann, S., Hoppe, P. and Herrmann, H.: In-cloud sulfate addition to single particles resolved with sulfur isotope analysis during HCCT-2010, Atmos. Chem. Phys., 14, 4219-4235, doi:10.5194/acp-14-4219-2014, 2014.

Hammer, E., Gysel, M., Roberts, G.C., Elias, T., Hofer, J., Hoyle, C.R., Bukowiecki, N., Dupont, J.C., Burnet, F., Baltensperger, U. and Weingartner, E.: Size-dependent particle activation properties in fog during the ParisFog 2012/13 field campaign, Atmos. Chem. Phys., 14, 10517-10533, 2014.

Hayden, K. L., Macdonald, A. M., Gong, W., Toom-Sauntry, D., Anlauf, K. G., Leithead, A., Li, S. M., Leaitch, W. R. and Noone, K.: Cloud processing of nitrate, J. Geophys. Res. Atmos., 113(D18), doi:10.1029/2007jd009732, 2008.

Herckes, P., Valsaraj, K.T. and Collett, J.L., A review of observations of organic matter in fogs and clouds: Origin, processing and fate, Atmos. Res., 132, 434-449. 2013.

Hiranuma, N., Brooks, S. D., Moffet, R. C., Glen, A., Laskin, A., Gilles, M. K., Liu, P., Macdonald, A.M., Strapp, J.W. and McFarquhar, G. M.: Chemical characterization of individual particles and residuals of cloud droplets and ice crystals collected on board

668 research aircraft in the ISDAC 2008 study, J. Geophys. Res. Atmos., 118(12), 6564-
669 6579, 2013.
670 Hudson, P.K., Murphy, D.M., Cziczo, D.J., Thomson, D.S., de Gouw, J.A., Warneke, C.,
671 Holloway, J., Jost, H.J. and Hübler, G.: Biomass-burning particle measurements:
672 Characteristic composition and chemical processing, J. Geophys. Res. Atmos., 109,
673 D23S27, doi:10.1029/2003JD004398, 2004.
674 Kamphus, M., Ettner-Mahl, M., Klimach, T., Drewnick, F., Keller, L., Cziczo, D. J.,
675 Mertes, S., Borrmann, S. and Curtius, J.: Chemical composition of ambient aerosol, ice
676 residues and cloud droplet residues in mixed-phase clouds: single particle analysis
677 during the Cloud and Aerosol Characterization Experiment (CLACE 6), Atmos. Chem.
678 Phys., 10, 8077-8095, doi:10.5194/acp-10-8077-2010, 2010.
679 Kleinman, L.I., Daum, P.H., Lee, Y.-N., Lewis, E.R., Sedlacek III, A., Senum, G.,
680 Springston, S., Wang, J., Hubbe, J. and Jayne, J.: Aerosol concentration and size
681 distribution measured below, in, and above cloud from the DOE G-1 during VOCALS-
682 Rex, Atmos. Chem. Phys., 12, 207-223, 2012.
683 Laskin, A., Moffet, R. C., Gilles, M. K., Fast, J. D., Zaveri, R. A., Wang, B., Nigge P.
684 and Shutthanandan, J.: Tropospheric chemistry of internally mixed sea salt and organic
685 particles: Surprising reactivity of NaCl with weak organic acids, J. Geophys. Res.
686 Atmos., 117(D15), doi:10.1029/2012JD017743, 2012.
687 Lee, C. S. L., Li, X., Zhang, G., Peng, X. and Zhang, L.: Biomonitoring of trace metals in
688 the atmosphere using moss (Hypnum plumaeforme) in the Nanling Mountains and the
689 Pearl River Delta, Southern China. Atmos. Environ., 39(3), 397-407, 2005.

690 Li, L., Huang, Z., Dong, J., Li, M., Gao, W., Nian, H., Fu, Z., Zhang, G., Bi, X. and
691 Cheng, P.: Real time bipolar time-of-flight mass spectrometer for analyzing single
692 aerosol particles, Int. J. Mass Spectrom., 303, 118-124,
693 doi:http://dx.doi.org/10.1016/j.ijms.2011.01.017, 2011a.
694 Li, T., Wang, Y., Zhou, J., Wang, T., Ding, A., Nie, W., Xue, L., Wang, X. and Wang,
695 W.: Evolution of trace elements in the planetary boundary layer in southern China:
696 effects of dust storms and aerosol-cloud interaction, J. Geophys. Res. Atmos., 122,
697 3492-3506, 2017.
698 Li, W., Li, P., Sun, G., Zhou, S., Yuan, Q. and Wang, W.: Cloud residues and interstitial
699 aerosols from non-precipitating clouds over an industrial and urban area in northern
700 China, Atmos. Environ., 45, 2488-2495, doi:10.1016/j.atmosenv.2011.02.044, 2011b.
701 Lohmann, U., Stier, P., Hoose, C., Ferrachat, S., Kloster, S., Roeckner, E. and Zhang, J.:
702 Cloud microphysics and aerosol indirect effects in the global climate model ECHAM5-
703 HAM, Atmos. Chem. Phys., 7, 3425-3446, 2007.
704 Matsuki, A., Schwarzenboeck, A., Venzac, H., Laj, P., Crumeyrolle, S. and Gomes, L.:
705 Cloud processing of mineral dust: direct comparison of cloud residual and clear sky
706 particles during AMMA aircraft campaign in summer 2006, Atmos. Chem. Phys., 10,
707 1057-1069, 2010.
708 McFiggans, G., Artaxo, P., Baltensperger, U., Coe, H., Facchini, M. C., Feingold, G.,
709 Fuzzi, S., Gysel, M., Laaksonen, A. and Lohmann, U.: The effect of physical and
710 chemical aerosol properties on warm cloud droplet activation, Atmos. Chem. Phys., 6,
711 2593-2649, doi:10.5194/acp-6-2593-2006, 2006.

McMeeking, G. R., Good, N., Petters, M. D., McFiggans, G. and Coe, H.: Influences on the fraction of hydrophobic and hydrophilic black carbon in the atmosphere, Atmos. Chem. Phys., 11(10), 5099-5112, 2011.

Medina, J., Nenes, A., Sotiropoulou, R. E. P., Cottrell, L. D., Ziemba, L. D., Beckman, P. J. and Griffin, R. J.: Cloud condensation nuclei closure during the International Consortium for Atmospheric Research on Transport and Transformation 2004 campaign: Effects of size-esolved composition, J. Geophys. Res. Atmos., 112(D10S31), doi:10.1029/2006JD007588, 2007.

Mertes, S., Lehmann, K., Nowak, A., Massling, A. and Wiedensohler, A.: Link between aerosol hygroscopic growth and dropletactivation observed for hill-capped clouds at connected flow conditions during FEBUKO, Atmos. Environ., 39, 4247-4256, 2005.

Moffet, R.C., Foy, B. D., Molina, L. A., Molina, M. and Prather, K.A.: Measurement of ambient aerosols in northern Mexico City by single particle mass spectrometry, Atmos. Chem. Phys., 8, 4499-4516, doi:10.5194/acp-8-4499-2008, 2008.

Moffet, R.C. and Prather, K.A.: In-situ measurements of the mixing state and optical properties of soot with implications for radiative forcing estimates, Proc. Natl. Acad. Sci. USA, 106, 11872-11877, doi: 10.1073/pnas.0900040106, 2009.

Moore, K. F., Sherman, D. E., Reilly, J. E. and Collett, J. L.: Drop size-dependent chemical composition in clouds and fogs. Part I. Observations, Atmos. Environ., 38(10), 1389-1402, 2004.

Moteki, N., Adachi, K., Ohata, S., Yoshida, A., Harigaya, T., Koike, M. and Kondo, Y.: Anthropogenic iron oxide aerosols enhance atmospheric heating, Nature Commun., 8, 15329, doi: 10.1038/ncomms15329, 2017.

735 Pratt, K.A., DeMott, P.J., French, J.R., Wang, Z., Westphal, D.L., Heymsfield, A.J.,
736 Twohy, C.H., Prenni, A.J. and Prather, K.A.: In situ detection of biological particles in
737 cloud ice-crystals, Nature Geos., 2, 398-401, 2009a.
738 Pratt, K.A., Hatch, L. E. and Prather, K. A.: Seasonal volatility dependence of ambient
739 particle phase amines, Environ. Sci. Technol., 43, 5276-5281, doi:10.1021/es803189n,
740 2009b.
741 Pratt, K.A., Heymsfield, A. J., Twohy, C. H., Murphy, S. M., DeMott, P. J., Hudson, J.
742 G., Subramanian, R., Wang, Z., Seinfeld, J. H. and Prather, K. A.: In Situ Chemical
743 Characterization of Aged Biomass-Burning Aerosols Impacting Cold Wave Clouds, J.
744 Atmos. Sci., 67, 2451-2468, doi:10.1175/2010jas3330.1, 2010a.
745 Pratt, K.A., Murphy, S., Subramanian, R., DeMott, P., Kok, G., Campos, T., Rogers, D.,
746 Prenni, A., Heymsfield, A. and Seinfeld, J.: Flight-based chemical characterization of
747 biomass burning aerosols within two prescribed burn smoke plumes, Atmos. Chem.
748 Phys., 11, 12549-12565, doi:10.5194/acp-11-12549-2011, 2011.
749 Pratt, K.A., Twohy, C.H., Murphy, S.M., Moffet, R.C., Heymsfield, A.J., Gaston, C.J.,
750 DeMott, P.J., Field, P.R., Henn, T.R., Rogers, D.C., Gilles, M.K., Seinfeld, J.H. and
751 Prather, K.A.: Observation of playa salts as nuclei in orographic wave clouds, J.
752 Geophys. Res. Atmos., 115, D15301, doi:10.1029/2009JD013606, 2010b.
753 Qin, X., Bhave, P.V. and Prather, K. A.: Comparison of two methods for obtaining
754 quantitative mass concentrations from aerosol time-of-flight mass spectrometry
755 measurements, Anal. Chem., 78(17), 6169-6178, doi: 10.1021/ac060395q, 2006.

Rehbein, P. J., Jeong, C. H., McGuire, M. L., Yao, X., Corbin, J. C. and Evans, G. J.: Cloud and fog processing enhanced gas-to-particle partitioning of trimethylamine, Environ. Sci. Technol., 45, 4346-4352, doi:10.1021/es1042113, 2011.

Rosenfeld, D., Lohmann, U., Raga, G.B., O'Dowd, C.D., Kulmala, M., Fuzzi, S., Reissell, A. and Andreae, M.O.: Flood or drought: how do aerosols affect precipitation?, Science, 321, 1309-1313, doi: 10.1126/science.1160606, 2008.

Roth, A., Schneider, J., Klimach, T., Mertes, S., van Pinxteren, D., Herrmann, H. and Borrmann, S.: Aerosol properties, source identification, and cloud processing in orographic clouds measured by single particle mass spectrometry on a central European mountain site during HCCT-2010, Atmos. Chem. Phys., 16, 505-524, doi:10.5194/acp-16-505-2016, 2016.

Schneider, J., Mertes, S., van Pinxteren, D., Herrmann, H. and Borrmann, S.: Uptake of nitric acid, ammonia, and organics in orographic clouds: Mass spectrometric analyses of droplet residual and interstitial aerosol particles, Atmos. Chem. Phys., 17, 1571-1593, doi:10.5194/acp-17-1571-2017, 2017.

Seinfeld, J.H., Bretherton, C., Carslaw, K.S., Coe, H., DeMott, P.J., Dunlea, E.J., Feingold, G., Ghan, S., Guenther, A.B. and Kahn, R.: Improving our fundamental understanding of the role of aerosol-cloud interactions in the climate system, Proc. Natl. Acad. Sci. USA, 113, 5781-5790, doi: 10.1073/pnas.1514043113, 2016.

Sellegri, Laj, P., Dupuy, R., Legrand, M., Preunkert, S. and Putaud, J.P.: Size-dependent scavenging efficiencies of multicomponent atmospheric aerosols in clouds, J. Geophys. Res. Atmos., 108, 4334, doi:10.1029/2002JD002749, 2003a.

778 Sellegri, K., Laj, P., Marinoni, A., Dupuy, R., Legrand, M. and Preunkert, S.:
779 Contribution of gaseous and particulate species to droplet solute composition at the
780 Puy de Dôme, France, Atmos. Chem. Phys., 3, 1509-1522, doi:10.5194/acp-3-1509-
781 2003, 2003b.
782 Shingler, T., Dey, S., Sorooshian, A., Brechtel, F. J., Wang, Z., Metcalf, A., Coggon, M.,
783 Mülmenstädt, J., Russell, L. M., Jonsson, H. H. and Seinfeld, J. H.: Characterisation
784 and airborne deployment of a new counterflow virtual impactor inlet, Atmos. Meas.
785 Tech., 5, 1259-1269, doi:10.5194/amt-5-1259-2012, 2012.
786 Sjogren, S., Gysel, M., Weingartner, E., Baltensperger, U., Cubison, M. J., Coe, H.,
787 Zardini, A.A., Marcolli, C., Krieger, U.K. and Krieger Peter, T.: Hygroscopic growth
788 and water uptake kinetics of two-phase aerosol particles consisting of ammonium
789 sulfate, adipic and humic acid mixtures, J. Aerosol Sci., 38(2), 157-171, 2007.
790 Song, X.H., Hopke, P. K., Fergenson, D. P. and Prather, K. A.: Classification of single
791 particles analyzed by ATOFMS using an artificial neural network, ART-2A, Anal.
792 Chem., 71, 860-865, doi:10.1021/ac9809682, 1999.
793 Sorooshian, A., Ng, N. L., Chan, A. W. H., Feingold, G., Flagan, R. C. and Seinfeld, J. H.:
794 Particulate organic acids and overall water-soluble aerosol composition measurements
795 from the 2006 Gulf of Mexico Atmospheric Composition and Climate Study
796 (GoMACCS), J. Geophys. Res. Atmos., 112(D13), doi:10.1029/2007JD008537, 2007a.
797 Sorooshian, A., Lu, M. L., Brechtel, F. J., Jonsson, H., Feingold, G., Flagan, R. C. and
798 Seinfeld, J. H.: On the source of organic acid aerosol layers above clouds, Environ. Sci.
799 Technol., 41, 4647-4654, doi: 10.1021/es0630442, 2007b.

800 Stier, P., Feichter, J., Kinne, S., Kloster, S., Vignati, E., Wilson, J., Ganzeveld, L., Tegen,
801 I., Werner, M. and Balkanski, Y.: The aerosol-climate model ECHAM5-HAM, Atmos.
802 Chem. Phys., 5, 1125-1156, 2005.
803 Svenningsson, B., Rissler, J., Swietlicki, E., Mircea, M., Bilde, M., Facchini, M. C.,
804 Decesari, S., Fuzzi, S., Zhou, J., Mønster, J. and Rosenørn, T.: Hygroscopic growth
805 and critical supersaturations for mixed aerosol particles of inorganic and organic
806 compounds of atmospheric relevance, Atmos. Chem. Phys., 6(7), 1937-1952, 2006.
807 Tang, M., Cziczo, D. J. and Grassian, V. H.: Interactions of Water with Mineral Dust
808 Aerosol: Water Adsorption, Hygroscopicity, Cloud Condensation, and Ice Nucleation,
809 Chem. Rev., doi:10.1021/acs.chemrev.5b00529, 2016.
810 Targino, A.C., Krejci, R., Noone, K.J. and Glantz, P.: Single particle analysis of ice
811 crystal residuals observed in orographic wave clouds over Scandinavia during
812 INTACC experiment, Atmos. Chem. Phys., 6, 1977-1990, 2006.
813 Tsai, J.H., Lin, K.H., Chen, C.Y., Ding, J.Y., Choa, C.G. and Chiang, H.L.: Chemical
814 constituents in particulate emissions from an integrated iron and steel facility, J.
815 Hazard. Mater., 147, 111-119, 2007.
816 Twohy, C.H., Kreidenweis, S.M., Eidhammer, T., Browell, E.V., Heymsfield, A.J.,
817 Bansemer, A.R., Anderson, B.E., Chen, G., Ismail, S., DeMott, P.J. and Van Den
818 Heever, S.C.: Saharan dust particles nucleate droplets in eastern Atlantic clouds,
819 Geophys. Res. Lett., 36, doi: 10.1029/2008GL035846, 2009.
820 Twohy, C.H. and Poellot, M.: Chemical characteristics of ice residual nuclei in anvil
821 cirrus clouds: evidence for homogeneous and heterogeneous ice formation, Atmos.
822 Chem. Phys., 5, 2289-2297, 2005.

Twohy C.H. and Anderson J. R.: Droplet nuclei in non-precipitating clouds: composition and size matter. Environ. Res. Lett., 3, 045002, doi:10.1088/1748-9326/3/4/045002, 2008.

Wang, H., An, J., Shen, L., Zhu, B., Xia, L., Duan, Q. and Zou, J.: Mixing state of ambient aerosols in Nanjing city by single particle mass spectrometry, Atmos. Environ., 132, 123-132, 2016.

Wang, Y., Guo, J., Wang, T., Ding, A., Gao, J., Zhou, Y., Collett, J. L. and Wang, W.: Influence of regional pollution and sandstorms on the chemical composition of cloud/fog at the summit of Mt. Taishan in northern China, Atmos. Res., 99, 434-442, doi:10.1016/j.atmosres.2010.11.010, 2011.

Wiedensohler, A., Cheng, Y. F., Nowak, A., Wehner, B., Achtert, P., Berghof, M., Birmili, W., Wu, Z. J., Hu, M., Zhu, T., Takegawa, N., Kita, K., Kondo, Y.,Lou, S. R., Hofzumahaus, A., Holland, F., Wahner, A., Gunthe, S. S., Rose, D., Su, H. and Takegawa, N.: Rapid aerosol particle growth and increase of cloud condensation nucleus activity by secondary aerosol formation and condensation: A case study for regional air pollution in northeastern China, J. Geophys. Res. Atmos., 114(D2), doi:10.1029/2008JD010884, 2009.

Wise, M. E., Surratt, J. D., Curtis, D. B., Shilling, J. E. and Tolbert, M. A. Hygroscopic growth of ammonium sulfate/dicarboxylic acids, J. Geophys. Res. Atmos., 108(D20), doi:10.1029/2003JD003775, 2003.

Zelenyuk, A., Imre, D., Earle, M., Easter, R., Korolev, A., Leaitch, R., Liu, P., Macdonald, A. M., Ovchinnikov, M. and Strapp, W.: In Situ Characterization of Cloud Condensation Nuclei, Interstitial, and Background Particles Using the Single Particle

Mass Spectrometer, SPLAT II†, Anal. Chem., 82, 7943-7951, doi:10.1021/ac1013892, 2010.

Zhang, R.Y., Khalizov, A. F., Pagels, J., Zhang, D., Xue, H. and McMurry, P. H.: Variability in morphology, hygroscopicity, and optical properties of soot aerosols during atmospheric processing, Proc. Natl. Acad. Sci. USA, 105, 10291-10296, doi:10.1073/pnas.0804860105, 2008.

Zhang, G., Bi, X., Chan, L. Y., Li, L., Wang, X., Feng, J., Sheng, G., Fu, J., Li, M. and Zhou, Z.: Enhanced trimethylamine-containing particles during fog events detected by single particle aerosol mass spectrometry in urban Guangzhou, China, Atmos. Environ., 55, 121-126, doi:10.1016/j.atmosenv.2012.03.038, 2012a.

Zhang, G., Bi, X., Li, L., Chan, L. Y., Li, M., Wang, X., Sheng, G., Fu, J. and Zhou, Z.: Mixing state of individual submicron carbon-containing particles during spring and fall seasons in urban Guangzhou, China: a case study, Atmos. Chem. Phys., 13, 4723-4735, doi:10.5194/acp-13-4723-2013, 2013.

Zhang, G., Bi, X., Lou, S., Li, L., Wang, H., Wang, X., Zhou, Z., Sheng, G., Fu, J. and Chen, C.: Source and mixing state of iron-containing particles in Shanghai by individual particle analysis, Chemosphere, 95, 9-16, 2014.

Zhang, G., Lin, Q., Peng, L., Bi, X., Lei, M., Chen, D., Brechtel, F.J., Chen, X., Yan, W.,Wang, X., Peng, P., Sheng., G. and Zhou, Z.: Single particle mixing state and cloud scavenging of black carbon at a high-altitude mountain site in south China, J. Geophys. Res. Atmos., in revise, 2017.

Zhang, X., Wang, Y., Niu, T., Zhang, X., Gong, S., Zhang, Y. and Sun, J.: Atmospheric aerosol compositions in China: spatial/temporal variability, chemical signature,

869 regional haze distribution and comparisons with global aerosols, Atmos. Chem. Phys.,
870 12, 779-799, doi:10.5194/acp-12-779-2012, 2012b.
871 Zhang, Y.P., Wang, X.F., Chen, H., Yang, X., Chen, J.M. and Allen, J.O.: Source
872 apportionment of lead-containing aerosol particles in Shanghai using single particle
873 mass spectrometry, Chemosphere, 74, 501-507, 2009.

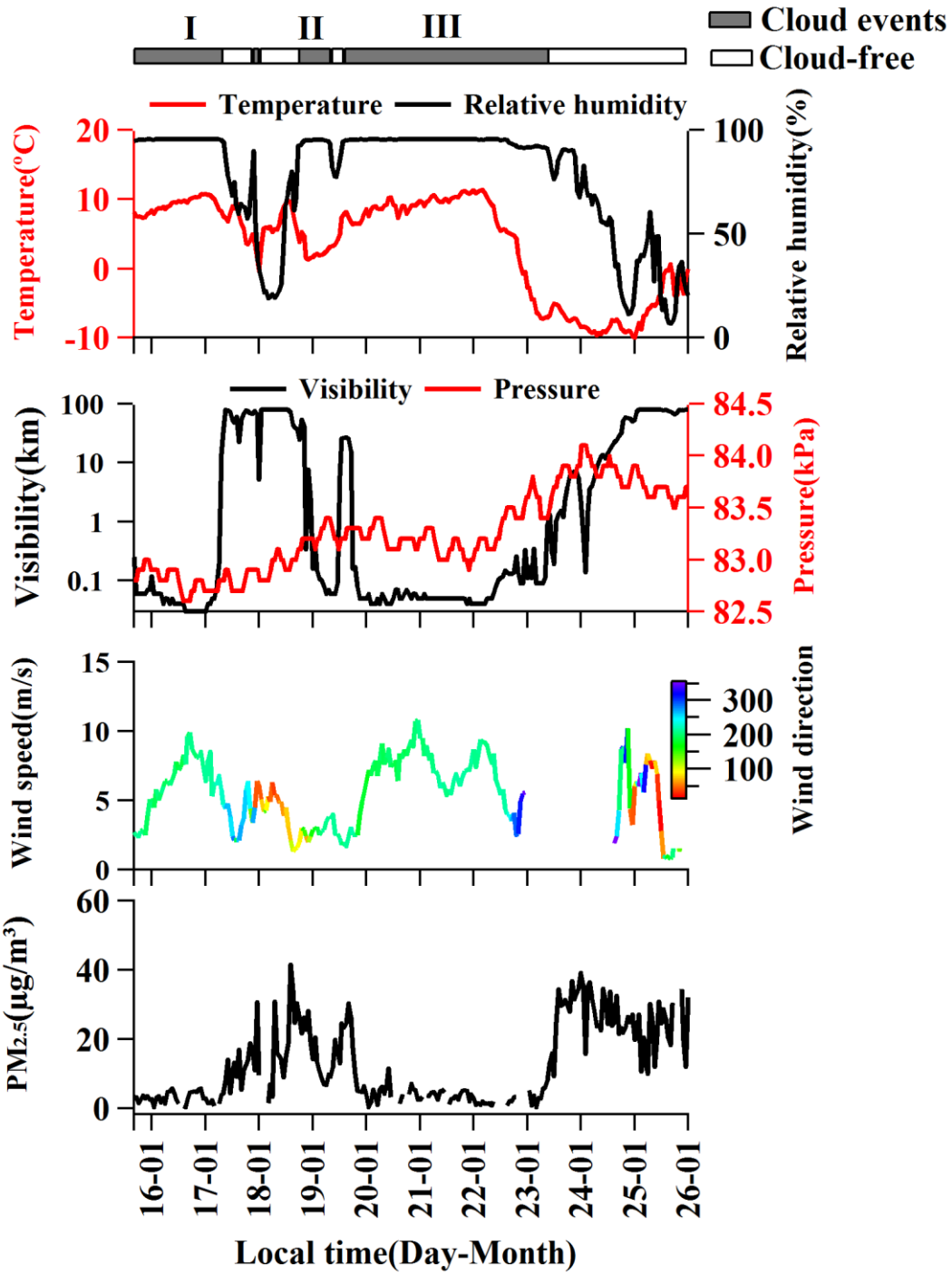

875

876 Figure 1: The hourly average variations in meteorological conditions (temperature,

877 relative humidity, visibility, pressure, wind speed and direction) and $PM_{2.5}$.

878

879 (a)

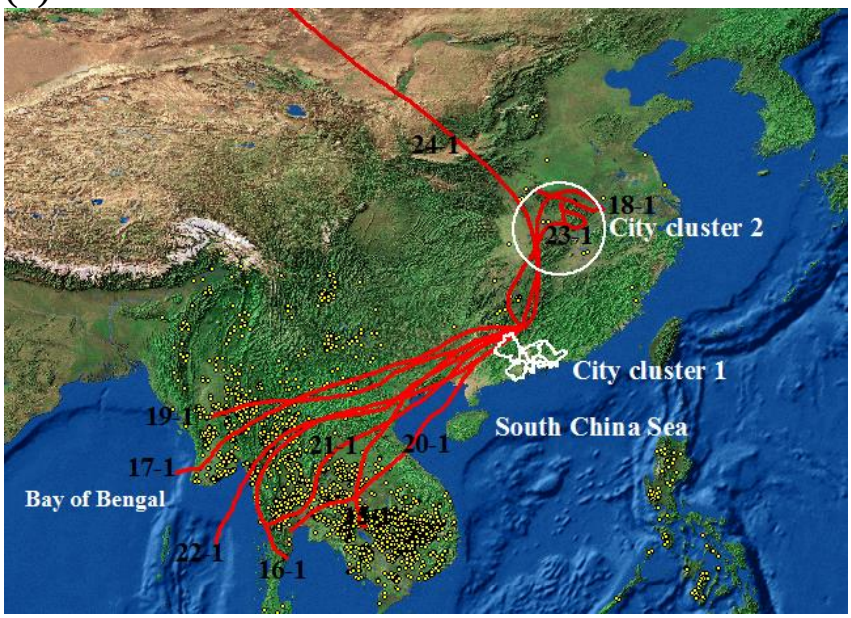

880

881 (b)

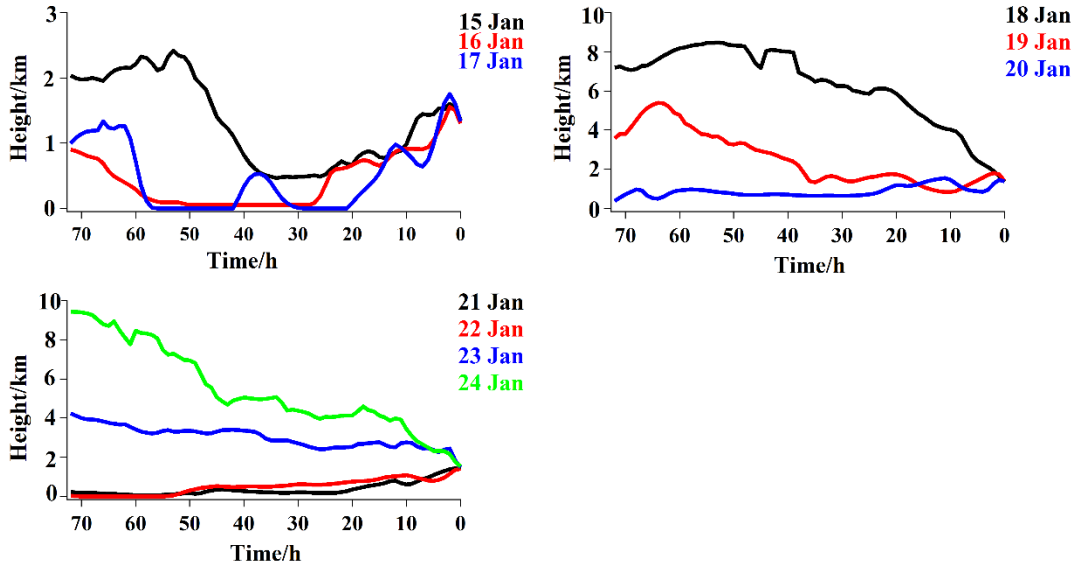

882

883 Figure 2: (a) HYSPLIT back trajectories (72 h) for air masses at 1,800 m during the
884 whole sampling period. The white borders and circle refer to the Pearl River Delta (city
885 cluster 1) and Yangtze River Mid-Reaches city clusters (city cluster 2), respectively. The
886 fire date (yellow dots) are available at https://earthdata.nasa.gov/; (b) Heights (above
887 model ground) of the air masses as a function of time.

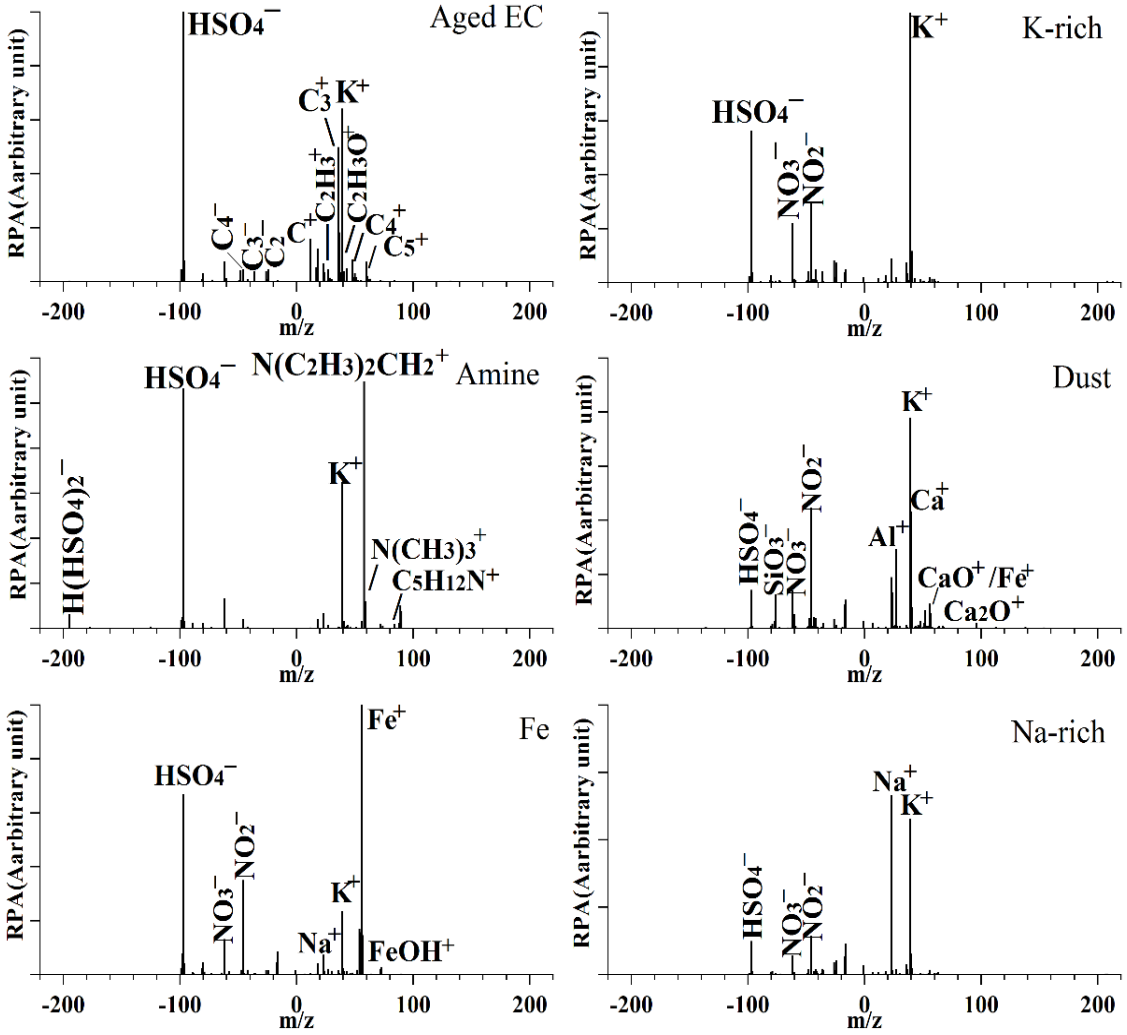

Figure 3: Averaged positive and negative mass spectra for the main 6 particle types (Aged EC, K-rich, Amine, Dust, Fe, Na-rich) of the sampled particles. RPA in the vertical axis refers to relative peak area. m/z in the horizontal axis represents mass-to-charge ratio.

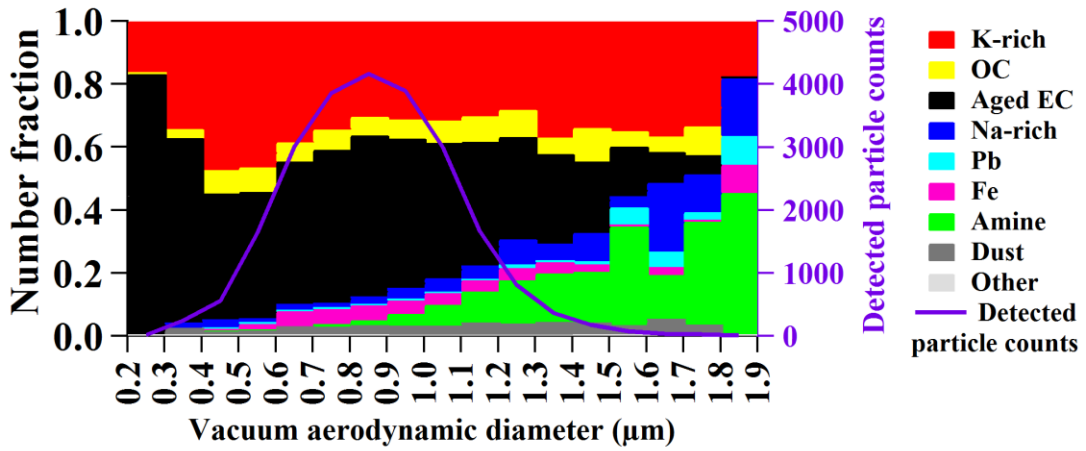

894

895 Figure 4: Number fraction for size distribution of the cloud residual types in 100 nm size

896 intervals.

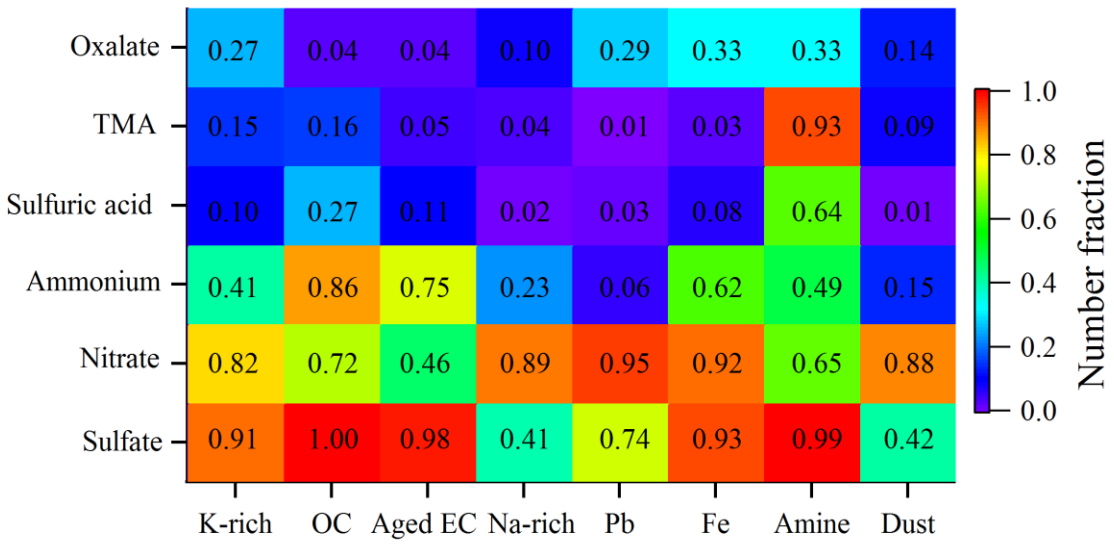

897

898 Figure 5: Number fraction of secondary markers associated with the total cloud residues

899 types; Sulfate (m/z, -97HSO_4^-), Nitrate (m/z, -46NO_2^- or -62NO_3^-), Ammonium (m/z,

900 18NH_4^+), Sulfuric acid (m/z, -195$H(HSO_4)_2^-$), TMA (m/z, 59$N(CH_3)_3^+$), Oxalate (m/z, -

901 89$HC_2O_4^-$).

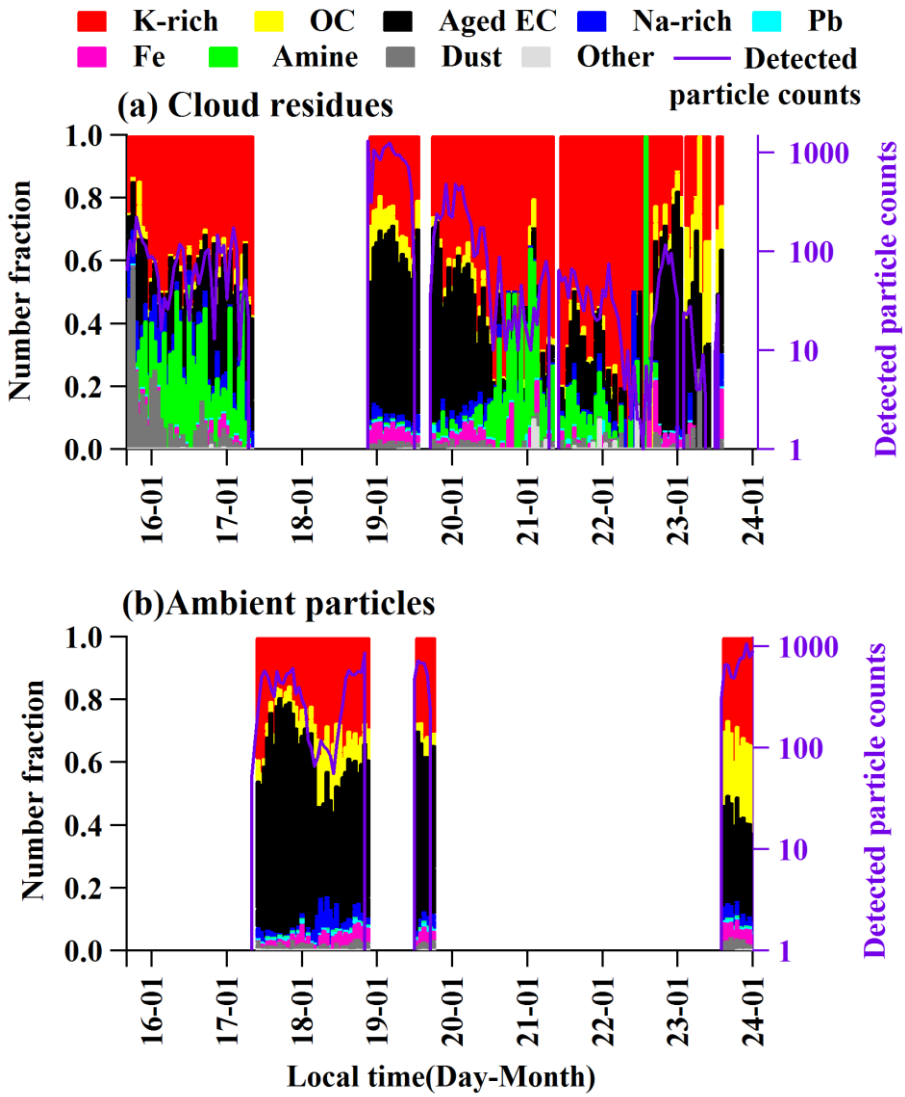

902
903
904 Figure 6: The hourly average variations in the cloud residual and ambient particles during
905 the whole sampling period.

906

907

908

909

910

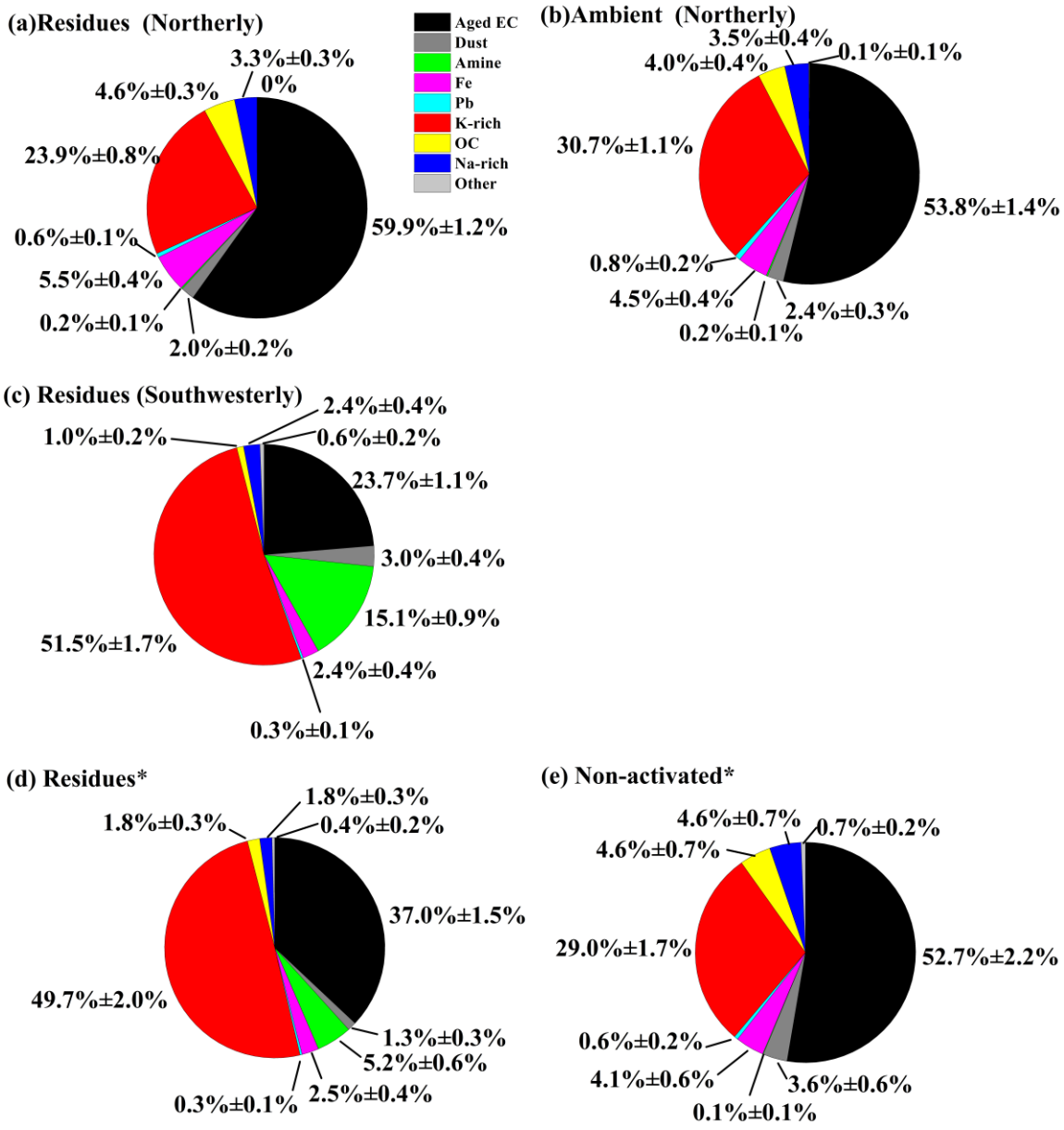

Figure 7: Number fraction of the cloud residues, ambient and non-activated particles. (a) cloud residues during northerly air mass; (b) ambient particle during northerly air mass; (c) cloud residues during southwesterly air mass; (d) cloud residues and (e) non-activated particles were alternately sampled with an interval of one hour during cloud III event. Uncertainties were calculated assuming Poisson statistics for analyzed particles.

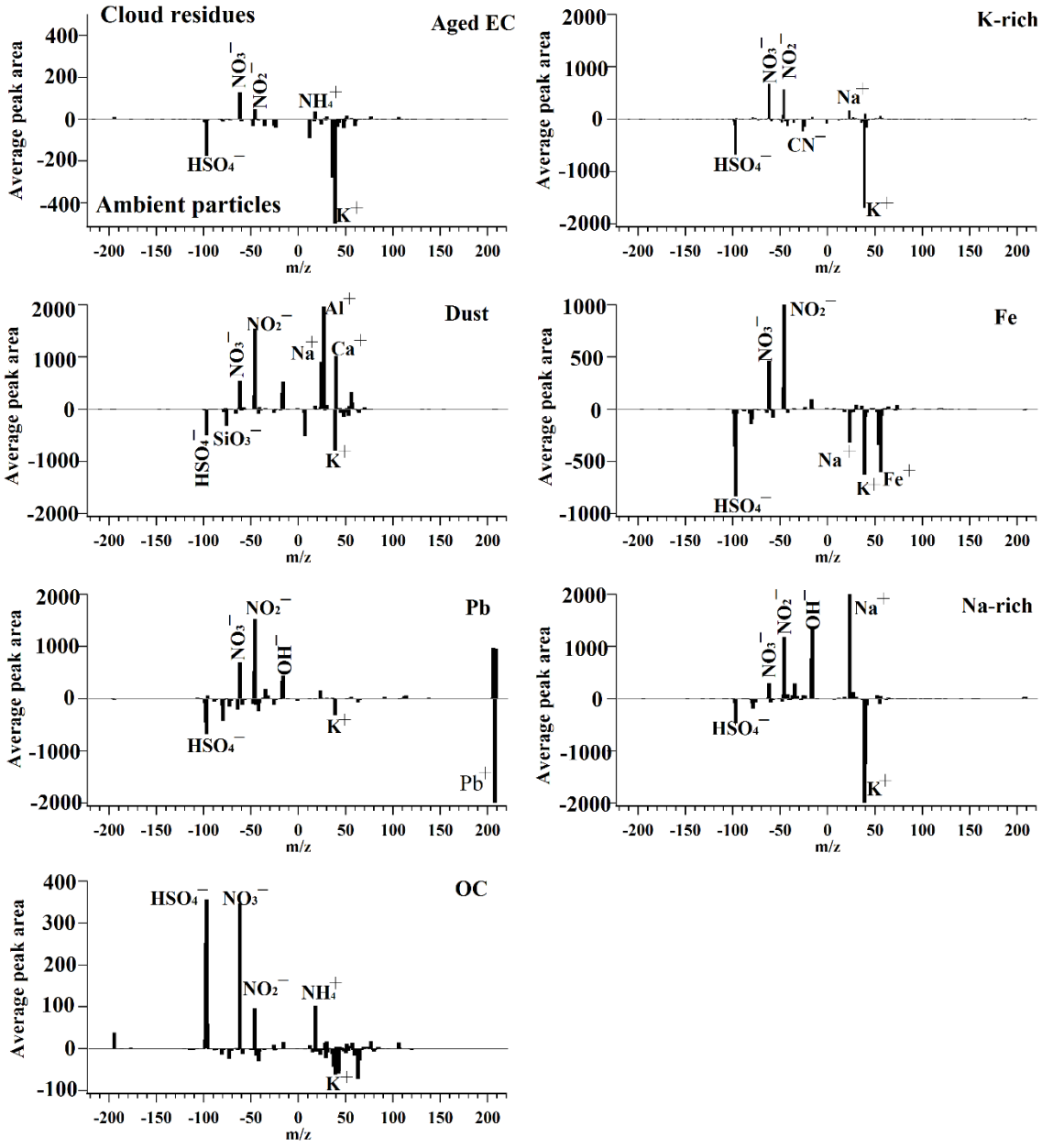

Figure 8: Mass spectral subtraction plot of the average mass spectrum corresponding to cloud residues minus ambient particles. Positive area peaks correspond to higher abundance in cloud residues; whereas, negative area peaks show higher intensity in ambient particles.

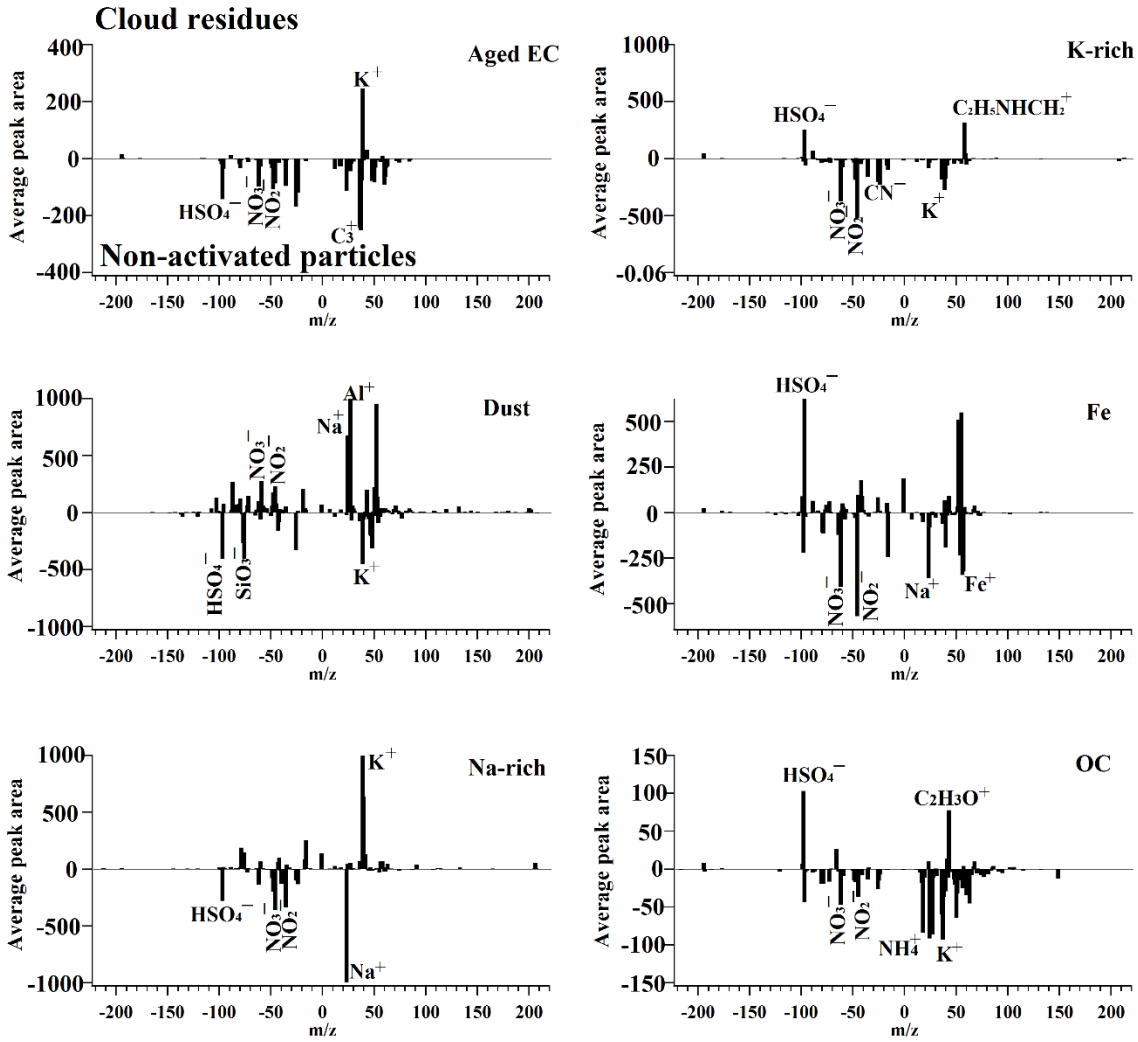

Figure 9: Mass spectral subtraction plot of the average mass spectrum corresponding to cloud residues minus non-activated particles. Positive area peaks correspond to higher abundance in cloud residues; whereas, negative area peaks show higher intensity in non-activated particles.